Optical and redox properties of *meso*-diphenyltetrabenzoporphyrins

Madoka Yasuike*, Tsuguo Yamaoka
Department of Image Science and Technology, Faculty of Engineering, Chiba University, 1-33 Yayoi-cho, Chiba 260 (Japan)

Osamu Ohno
Department of Chemistry, Faculty of Science, Tokyo Institute of Technology, 2-12-1 Ookayama, Meguro-ku, Tokyo 152 (Japan)

Kunihiro Ichimura, Hisayuki Morii and **Masako Sakuragi**
Research Institute for Polymers and Textiles, 1-1-4 Higashi, Tsukuba, Ibaraki 305 (Japan)

(Received January 14, 1991)

Abstract

The *meso*-diphenyltetrabenzoporphyrin zinc complex (**1b**, ZnP_2TBP) having two phenyl substituents at the neighboring *meso*-positions was isolated by the careful purification of the reaction product of 3-benzylidenephthalimidine (3-BPI) with zinc acetate. The treatment of **1b** with trifluoroacetic acid led to the successful demetalation of **1b** to its metal free compound (**1e**, H_2P_2TBP). Hence, the other divalent metallic complexes such as magnesium (**1a**), cadmium (**1c**) and palladium (**1d**) were readily prepared by metal insertion into **1e** with the appropriate metal sources. The well-defined structural elucidation of these *meso*-diphenyltetrabenzoporphyrins (P_2TBP) has enabled us to determine their electrochemical and optical properties. Among the metallo P_2TBPs discussed here, the Mg complex possesses both the lowest oxidation and reduction potentials whilst the Pd complex has the highest oxidation and reduction potentials. This result was explained on the basis of the induction effect on the porphyrin ring current by the central metal ion. The absorption maxima of these metallo P_2TBPs were also affected by the central metal ions. Since these TBPs reasonably fluoresce at room temperature and phosphoresce at 77 K as in the case of the corresponding metallotetraphenylporphyrins (TPP), their excited state energies were measurable. Their fluorescence quantum yields (Φ_f) and lifetimes (τ_f) obeyed the heavy atom effect by the central metal ions. Finally, we also discussed their redox properties in the excited states.

Introduction

Metalloporphyrins play an important role with respect to many biological enzymic functions, such as photosynthesis, redox reactions, and the fixation and transport of oxygen [1–3]. On the other hand, metallotetrabenzoporphyrins (TBP) have been attracting interest as a chlorophyll-like compound from the viewpoints of both the absorption properties in the long wavelength region [4] and their redox properties [5], because their Q bands lie on the red light wavelength region with high extinction coefficients and the extension of the π-electron system of the porphyrin ring by the benzo-substitution at the β,β'-pyrrole carbon atoms of the porphyrin skeleton is expected to lead to a considerable decrease in the redox potentials [5a]. In spite of these unique optical and redox properties of TBPs, their poor solubilities in common organic solvents make them difficult to use in practical applications. To overcome this solubility problem, some efforts have been made on the preparation of the tetraphenyltetrabenzoporphyrin zinc complex (ZnP_4TBP) having four phenyl substituents at its *meso*-positions as in the case of tetraphenylporphyrin (TPP) [6a–d]. However, these attempts have unfortunately failed in the preparation of ZnP_4TBP as previously reported [7a,b]. Therefore, the lack of information on the structural elucidation of the *meso*-phenyl substituted TBP zinc complex (ZnPTBP) has posed difficulties in measuring their optical and electrochemical properties. Consequently, our study on the preparation and structural analyses of ZnPTBP has led to the successful isolation of ZnP_4TBP, ZnP_3TBP and ZnP_2TBP [7a]. In particular ZnP_2TBP (**1b**), whose two phenyl substituents were located at the neighboring *meso*-positions, was obtained as a chief product of the reaction of 3-BPI with zinc acetate. This has enabled us to prepare

*Author to whom correspondence should be addressed.

0020-1693/91/$3.50

the other metallo P_2TBPs by use of **1b** as a well-defined starting material and correctly elucidate their various properties.

In the present work, we mainly report the optical and redox properties of the divalent metallo P_2TBP_2 including magnesium (**1a**), zinc (**1b**), cadmium (**1c**) and palladium (**1d**), and those for the metal free compound (**1e**) are also discussed.

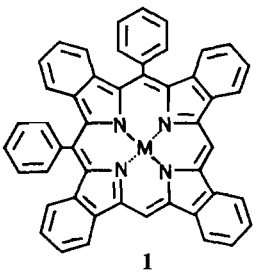

1

Structure of *meso*-diphenyltetrabenzoporphyrin: M = Mg (**1a**), Zn(**1b**), Cd(**1c**), Pd(**1d**), H_2(**1e**).

Experimental

Materials

meso-Diphenyltetrabenzoporphyrin zinc complex (ZnP_2TBP, 1b)

The *meso*-diphenyltetrabenzoporphyrin zinc complex (ZnP_2TBP, **1b**) was obtained by the reaction of 3-BPI in the presence of zinc acetate at 360 °C for 1 h under N_2, followed by careful purification with repeated column chromatography on alumina (Merck 1097) and TLC (Merck 5756) on alumina using a solvent mixture of benzene/hexane/THF (10/10/1 vol. ratio). The third green fraction band from the top fraction contained **1b**. This complex was contaminated with its benzyl adducts to some degree, as previously reported [7a]. ^1H–^1H COSY spectrum in acetone-d_6, δ in ppm: methine-H: 11.07 (2H); *meso*-phenyl Hs: 8.25 (*o*-Hs, 4H), 8.12 (*p*-Hs, 2H), 8.00 (*m*-Hs, 4H); benzene-ring Hs: 9.78 (4H), 8.20 (2H), 7.96 (2H), 7.59 (2H), 7.35 (2H), 7.28 (2H), 7.10 (2H). FD-MS: $m/z = 724$, 814, 904. UV–Vis in benzene (log ϵ): Soret bands: 408 (4.54), 432 (5.38); Q bands: 582 (4.02), 603 (5.01) nm.

Preparation of H_2P_2TBP (1e), MgP_2TBP (1a), CdP_2TBP (1c) and PdP_2TBP (1d)

The other metallo P_2TBPs, MgP_2TBP (**1a**), CdP_2TBP (**1c**) and PdP_2TBP (**1d**), and the metal free compounds, H_2P_2TBP (**1e**), were prepared as follows.

First, **1b** (0.34 g) was dissolved into chloroform (10 ml) and trifluoroacetic acid (7 ml) was gradually added at room temperature. After stirring for 3 h, the reaction mixture was poured into a 500 ml mixture of ethanol and water (1/1 vol. ratio) and then neutralized with anhydrous sodium carbonate. The resulting green compound in the solvent was filtered with suction and dried *in vacuo*. A repeated purification by TLC on alumina in a similar way as previously mentioned led to 0.29 g of H_2P_2TBP (**1e**).

FD-MS: $m/z = 662$, 752, 842. UV–Vis in benzene (log ϵ), Soret bands: 400 (4.46), 427 (5.16), 441 (5.30); Q bands: 533 (3.51), 574 (4.03), 614 (4.61), 672 (4.32) nm.

The metallo complexes were made by the metal ion insertion into **1e** using the appropriate metal salts. The reaction was completed when the absorption of **1e**, especially its splitting Q band, was changed to those of the metallic complexes. The Cd (**1c**) and Pd (**1e**) complexes were synthesized by the reaction of **1e** with an excess of the corresponding metal acetates in chloroform/metal (10/1 vol. ratio) under reflux followed by the evaporation of the solvent *in vacuo*. On the other hand, the production of the Mg (**1a**) complex was achievable by the metalation of **1e** in the presence of magnesium perchlorate pyridine for 6 h under reflux. The evaporation of the pyridine solution *in vacuo* led to a paste-like residue, which was then dissolved into a mixture of benzene/ether (1/1 vol. ratio). This solution was washed three times with 0.1 N HCl aq. solution and neutralized twice with a saturated sodium hydrogencarbonate aq. solution, and then dried over anhydrous magnesium sulfate. The evaporation of this solution gave **1a**. These metallo P_2TBPs were purified by repeated column chromatography and TLC in the same manner as in the case of the zinc complex (**1b**).

MgP_2TBP (**1a**): FD-MS: $m/z = 684$, 774, 864. UV–Vis in benzene (log ϵ): Soret bands: 412 (4.64), 436 (5.53), Q bands: 590 (4.11), 636 (5.03) nm.

CdP_2TBP (**1c**): FD-MS: $m/z = 774$, 864, 954. UV–Vis in benzene (log ϵ): Soret bands: 420 (4.65), 444 (5.51); Q bands: 590 (4.17), 634 (5.01) nm.

PdP_2TBP (**1d**): FD-MS: $m/z = 766$, 854, 944. UV–Vis in benzene (log ϵ): Soret bands: 398 (4.31), 422 (5.27), 475 (3.99); Q bands: 565 (4.01), 615 (5.01), 726 (2.60) nm.

Physical measurements

The structural analyses were carried out with a Hitachi M-80 field-desorption mass spectrometer (FD-MS) and a NICOLET NT-360NB nuclear magnetic resonance spectrometer.

The redox potentials were determined in DMF containing 0.1 M tetra-n-butylammonium perchlorate as an electrolyte by cyclic voltammetry on a HOKUTO DENKO HB-104 function generator and HB-501 potentiostat/galvanostat with a Yokogawa 3086

X-Y recorder, utilizing a three electrode system (stationary platinum, platinum wire auxiliary and Ag/$AgClO_4$ reference electrode). The scanning voltage was 100 mV s^{-1}.

Ultraviolet and visible spectra (UV–Vis) were obtained on a JASCO Ubest-30 spectrophotometer. Fluorescence and phosphorescence measurements were carried out on a JASCO 770FP spectrofluorometer equipped with a red-sensitive photomultiplier (Hamamatsu Photonics R928). Fluorescence spectra and the quantum yields relative to ZnTPP in benzene ($\Phi_f = 0.033$) [8] were obtained from the optically diluted benzene solutions (10^{-6} M) after a thorough purging with argon gas. Phosphorescence spectra were recorded in frozen EPA glasses at 77 K prepared by thorough purging with argon gas.

Fluorescence lifetimes were recorded at 20 °C in the optically diluted benzene solutions (10^{-6} M) prepared through purging with argon gas using a conventional time-correlated single photon counting method with HORIBA NAES-1100.

Results and discussion

Structural analyses of ZnP_2TBP (1b) and the other P_2TBPs

As previously reported [7a], the reaction of 3-BPI with zinc acetate provided a complicated mixture of *meso*-phenyl substituted tetrabenzoporphyrin zinc complexes (ZnPTBP) including ZnP_4TBP, ZnP_3TBP, ZnP_2TBP and ZnP_1TBP. Moreover, these ZnPTBP products were contaminated with the additional compounds to which the benzyl group(s) were attached. In the case of ZnP_2TBP, the existence of two isomers which are different in the location of the two *meso*-phenyl substituents can be considered to be obtained. Figure 1 shows the sets of ^1H NMR and ^1H–^1H COSY spectra of ZnP_2TBP in acetone-d_6, where the structure of one of two ZnP_2TBP isomers whose two phenyl groups are positioned at the neighboring *meso*-positions is exactly established as follows. (a) The two *meso*-Hs (the 17 and 18 positions) are detected as a singlet at a considerably low magnetic field of 11.07 ppm. This remarkable deshielding effect on the chemical shift is caused by the porphyrin ring current. (b) Another proton signal at low magnetic field of 9.78 ppm is also observed. ^1H NMR of ZnTBP has revealed that the inner Hs on the benzene rings appear in the lower magnetic region compared to those of the outer Hs [6d, 7b]. Thus, this proton signal is assignable to the Hs for the 1, 4, 5 and 16 positions on the benzene ring. This assignment is certainly substantiated by the following fact. The Hs at the 1 and 4 positions are coupled with those at the 2 and 3 positions. On the other hand, the Hs at the 5 and 16 positions are coupled with a series of the Hs on the benzene rings, that is, the 6 and 15 Hs at 7.96 ppm, the 7 and 14 Hs at 7.59 ppm, and the 8 and 13 Hs at 7.10 ppm. The reason why the 8 and 13 Hs are shifted to the higher magnetic field in comparison with the 7 and 14 Hs is due to the shielding effect by the *meso*-phenyl substituents which are probably out of the plane of the macrocycle on account of the steric hindrance. (c) The sets of the 9, 12 Hs and the 10, 11 Hs on the benzene ring

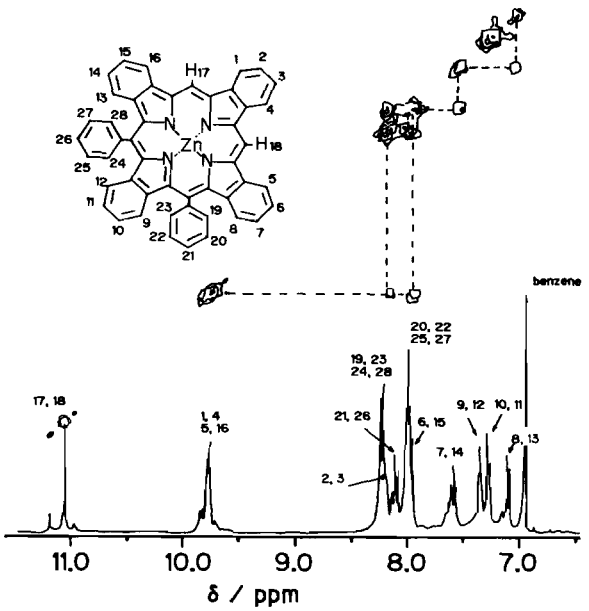

Fig. 1. ^1H NMR and ^1H–^1H COSY spectra of ZnP_2TBP recorded at 360 MHz in acetone-d_6. The numbers in the ^1H NMR spectrum correspond to those for the Hs on the ZnP_2TBP structure. The dashed lines represent the relationship between the coupled proton pairs.

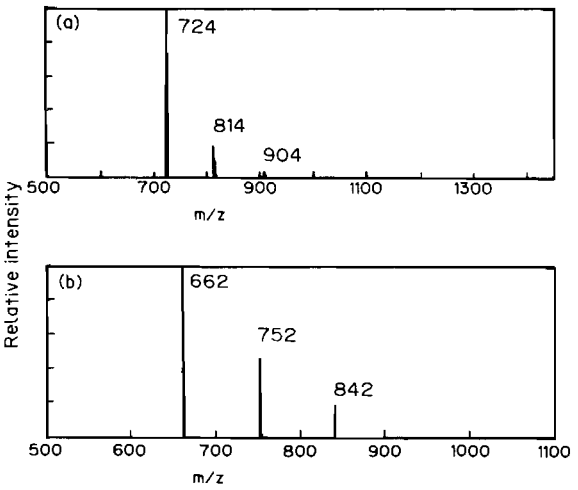

Fig. 2. Field desorption mass spectra (FD-MS) of: (a) ZnP_2TBP obtained by the reaction of 3-BPI with zinc acetate; (b) H_2P_2TBP prepared by the demetalation of ZnP_2TBP.

TABLE 1. FD-MS data of metallo P_2TBPs and H_2P_2TBP and their assignments

Compound	m/z		
MgP_2TBP (**1a**)	684[a],	774(684+90)[b],	864(684+90×2)[c]
ZnP_2TBP (**1b**)	724,	814(724+90),	904(724+90×2)
CdP_2TBP (**1c**)	774,	864(774+90),	954(774+90×2)
PdP_2TBP (**1d**)	766,	856(766+90),	946(766+90×2)
H_2P_2TBP (**1e**)	662,	752(662+90),	842(662+90×2)

[a]Mass ion peak of the parent molecule. [b],[c]Mass ion peak of the benzyl adduct.

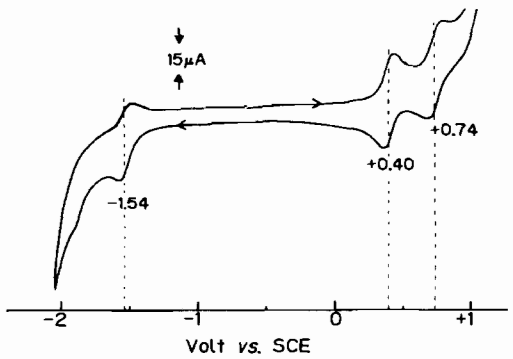

Fig. 3. Cyclic voltammogram of MgP_2TBP in DMF using three electrode system (stationary platinum, platinum wire auxiliary and $Ag/AgClO_4$ reference electrode) and 0.1 M of tetra-n-butylammonium perchlorate as an electrolyte. The scanning voltage was 100 mV s^{-1}. Two reversible oxidation steps and one reversible reduction step were observed.

which are interposed between the two *meso*-phenyl groups are detected at 7.35 and 7.28 ppm, respectively. These Hs are independent of the Hs on the other benzene rings. (d) The *meso*-phenyl protons (*o*, *m* and *p*-positions) are observed at 8.25, 8.00 and 8.12 ppm.

The ^1H NMR data provides conclusive proof that the ZnP_2TBP discussed here is one of the two isomers whose two phenyl groups are positioned at the neighboring *meso*-positions. However, as shown in Fig. 2, the FD-MS of this compound indicates contamination with the benzyl adduct(s) whose mass ion peaks are $m/z = 814$ and 904, respectively. Figure 2 also shows the FD-MS of the metal free compound, H_2P_2TBP (**1e**), where the mass ion peaks of $m/z = 752$ and 842 corresponding to the molecular weights of the benzyl adducts of H_2P_2TBP were also detected in addition to $m/z = 662$.

Considering the previous results for the structural elucidation of ZnP_2TBP and H_2P_2TBP, we should handle the other metallo P_2TBPs (**1a**, **1c** and **1d**), because they were obtained using **1e** as the starting material. Before mentioned with regard to the optical and electrochemical properties of the P_2TBPs, it should be noted that these P_2TBPs are contaminated with the benzyl adducts to some degree as well as ZnP_2TBP, as shown in the FD-MS data given in Table 1.

Redox properties of P_2TBPs in the ground state

Generally, it is well known that most of the diamagnetic porphyrin complexes, the so-called regular type or closed shell type of porphyrin, are reversibly either oxidized or reduced in two, sequential, one-electron steps, which are caused by the porphyrin ring current [9]. These two redox steps provide either the cation radical and dication species in the oxidation step, or the anion radical and dianon species in the reduction step, respectively. There is a relationship between the redox potentials of a conjugated π-

TABLE 2. Half-wave potentials of P_2TBPs in comparison with those for ZnTPP and ZnTBP, and the relationship between the gap of the first redox potential (ΔE) and the energy of the long wavelength ($h\nu$) in DMF

Compound	$E_{ox}^{1/2}$[a] vs. SCE		$E_{red}^{1/2}$[a] vs. SCE		ΔE[b]	$h\nu$[c]
	(II)	(I)	(I)	(II)		
MgP_2TBP (**1a**)	0.74	0.40	−1.54		1.94	1.96
ZnP_2TBP (**1b**)	0.86	0.53	−1.44	−1.71	1.97	1.97
CdP_2TBP (**1c**)	0.78	0.54	−1.44		1.98	1.94
PdP_2TBP (**1d**)		0.74	−1.27	−1.72	2.01	2.02
H_2P_2TBP (**1e**)	1.05	0.72	−1.18	−1.56	1.90	1.85
ZnTBP		0.38	−1.48		1.86	1.96
		(0.36)[d]	(−1.48)[d]		(1.84)	
ZnTPP	1.04	0.86	−1.35	−1.78	2.21	2.07

[a]Half-wave potentials in the oxidation and reduction steps recorded in DMF by cyclic voltammetry, using three electrode system (stationary platinum, platinum wire auxiliary and $Ag/AgClO_4$ reference electrode). [b]The gap between the first oxidation and reduction potentials. [c]The energy of the long wavelength band in DMF. [d]For these data Vogler's paper was referred to, ref. 5a.

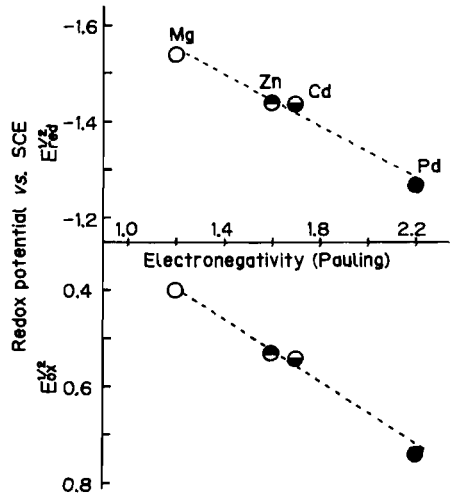

Fig. 4. Plots of the first oxidation and reduction potentials (vs. SCE) of metallo P_2TBPs in DMF as a function of the electronegativities (Pauling's data) of the central metals. ○, MgP_2TBP; ◓, ZnP_2TBP; ◒, CdP_2TBP; ●, PdP_2TBP.

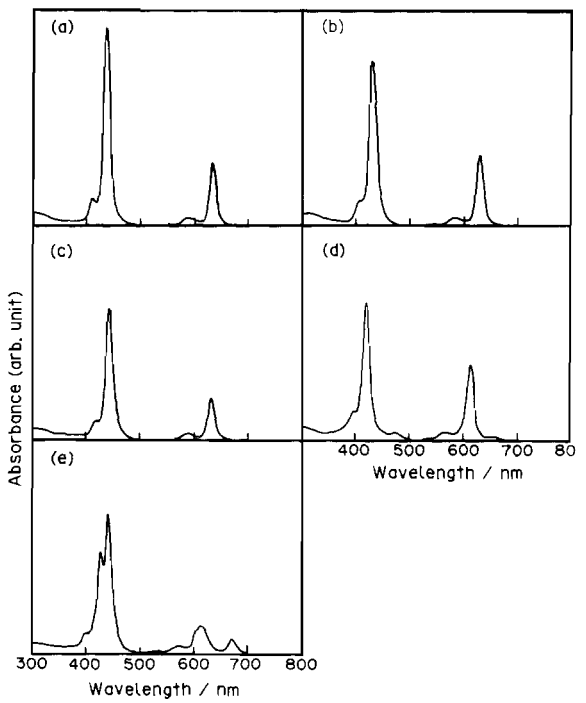

Fig. 5. A series of the ultraviolet and visible absorption spectra of P_2TBPs in benzene: (a) MgP_2TBP, (b) ZnP_2TBP, (c) CdP_2TBP, (d) PdP_2TBP, (e) H_2P_2TBP.

electron system and its absorption spectrum, that is, ΔE value $(E_{ox}-E_{red})=h\nu+0.01$, where $h\nu$ is the energy in electron volts of the long wavelength band [10]. Furhop *et al.* have reported that this relation has been found to hold approximately true and the difference in the redox potentials between the first-ring oxidation yielding π-cation radicals and the first reduction yielding π-anion radicals is in good agreement with the theoretically calculated value between the HOMO and LUMO in a number of metallo-octaethylporphyrins [11], as well as in the case of metallo TPPs [12]. Since the P_2TBPs dealt with in this paper exhibit reversible redox behaviors in their cyclic voltammograms in DMF, at least one of the two potentials in each redox step is measurable from their half-wave potentials in both the anodic and cathodic electrode processes. Figure 3 shows the cyclic voltammograms of MgP_2TBP (**1a**) as a typical case, where two reversible oxidation and one reversible reduction steps are demonstrated. Provided that the previous relationship between the gap in the redox potentials (ΔE) and the energy in the long wavelength absorption band ($h\nu$) can be expected to hold for the P_2TBPs discussed here, it is possible to determine their first redox potentials. The ΔEs between both the first anodic and cathodic half-wave potentials of **1a**, **1b**, **1c** and **1e** are approximately consistent with the energies of their Q bands in DMF solutions, as collected in Table 2. Although the Pd complex (**1d**) is not classified as a regular type of metalloporphyrin, this relationship is also found to hold. Hence, these half-wave potentials are assignable to the first oxidation and reduction potentials at which the π-cation and the π-anion radicals of the TBPs are probably produced. Table 2 summarizes their redox data (E_{ox} and E_{red}) in DMF solutions and the energies of their Q bands obtained from the same solvent, compared with those of ZnTPP and ZnTBP obtained under our experimental conditions.

Among the divalent complexes discussed here, the magnesium complex (MgP_2TBP) possesses the lowest first oxidation potential ($E_{ox}[1]$) of 0.40 V and the lowest first reduction potential ($E_{red}[1]$) of -1.55 V. Their $E_{ox}[1]$s increase in the following order: $MgP_2TBP < ZnP_2TBP < CdP_2TBP < PdP_2TBP$. On the other hand, their $E_{red}[1]$s also increase in the same order. The plots of either E_{ox}s or E_{red}s as a function of electronegativity of the central metals yield linear relationships as shown in Fig. 4. Both the oxidation and reduction potentials increase with increasing electronegativity of the central metals. The induction effect of the central metal on the π-electrons of the TBPs rings can explain these results.

Comparing the oxidation potential of ZnP_2TBP with that of either ZnTPP or ZnTBP measured under our experimental conditions, it is found that E_{ox} is lower than that of ZnTPP, while higher than that of ZnTBP, as shown in Table 2. The lowering of E_{ox} of ZnP_2TBP in comparison with that of ZnTPP is probably due to the extension of the π-electron system by benzo-substitution at the β,β'-pyrrole car-

TABLE 3. Absorption data for P_2TBPs in benzene solutions

Compound	λ_{max} (nm) (log ϵ)						
	Soret band			Q band			
MgP_2TBP (**1a**)	412(4.64)	436(5.53)		590(4.11)	636(5.03)		
ZnP_2TBP (**1b**)	408(4.54)	432(5.38)		582(4.02)	630(5.01)		
CdP_2TBP (**1c**)	420(4.65)	444(5.51)		590(4.17)	634(5.01)		
PdP_2TBP (**1d**)	398(4.31)	422(5.27)	475(3.99)	565(4.01)	615(5.01)	726(2.60)	
H_2P_2TBP (**1e**)	400(4.46)	427(5.16)	441(5.30)	533(3.51)	574(4.03)	614(4.61)	672(4.32)

TABLE 4. Relationship between the oscillator strength and the energy of the absorption bands (Soret or Q bands) in benzene

Compound	E(Q) ($\times 10^{-4}$ cm^{-1})[a]	f(Q)[b]	E(Soret) ($\times 10^{-4}$ cm^{-1})[c]	f(Soret)[d]
MgP_2TBP (**1a**)	1.572	0.16	2.294	1.13
ZnP_2TBP (**1b**)	1.587	0.17	2.315	0.94
CdP_2TBP (**1c**)	1.577	0.16	2.252	1.12
PdP_2TBP (**1d**)	1.626	0.20	2.370	0.84

[a]The energy of the lowest energy absorption band in wavelength. [b]The oscillator strength of the lowest energy absorption band. [c]The energy of the Soret band in wavenumber. [d]The oscillator strength of the Soret band.

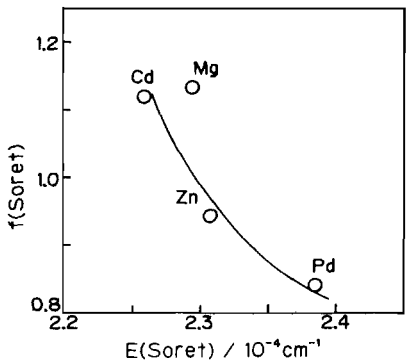

Fig. 6. Relationship between the oscillator strength (f) and the energy (E) of the Soret absorption band for metallo P_2TBPs.

bons, whilst E_{ox} is raised due to an electro-withdrawing effect on the TBP π-electron by the *meso*-phenyl substituents, compared with that of ZnTBP. This effect is supported by the fact that λ_{max} of ZnP_2TBP at both the Soret (447 nm) and Q bands (636 nm) are red-shifted in pyridine solution in comparison with those (Soret; 433 nm, Q; 628 nm) of ZnTBP. The red-shifting of the absorption bands is the effect of an electro-withdrawing by the *meso*-phenyl substituents [7a].

Optical properties of P_2TBP

Figure 5 shows a series of the UV–Vis absorption spectra of the P_2TBPs in benzene solutions. There is a little difference in λ_{max} of the Q bands among the Mg, Zn and Cd complexes. On the other hand, that of the Pd complex is drastically blue-shifted by *c.* 20 nm, compared with those of the others. Moreover, the additional absorption peaks of 475 and 726 nm with the relative low extinction coefficients are observed in the UV–Vis of the Pd complex. These absorption bands whose assignments are unclear appear even after repeated purification by TLC. All of the absorption data of the P_2TBPs are collected in Table 3.

Generally, the degree of the effect of the central metal ion on the absorption property of the metalloporphyrin depends on several factors including the size of the central metal ion, the geometry of the metalloporphyrin, and electrostatic and inductive effect. In the case of metallo TPPs, it is well known that the relationship between the oscillator strength (f_Q) and the energy (E_Q) of the lowest energy absorption band gives a simple evaluation for the degree of the interaction between the central metal ion and the porphyrin π-system, where with increased interaction the energy is raised and the oscillator strength is reduced [13]. For the oscillator strengths the following formula is used

$$f_Q = 4.315 \times 10^{-9} \int \epsilon d\nu$$

where ϵ and ν denote the extinction coefficient and absorption energy in wavelength. However, this relationship does not provide a convenient interpretation for the interaction between the central metal ions and the P_2TBP π-system because these metallo P_2TBPs are roughly identical in the calculated f_Q,

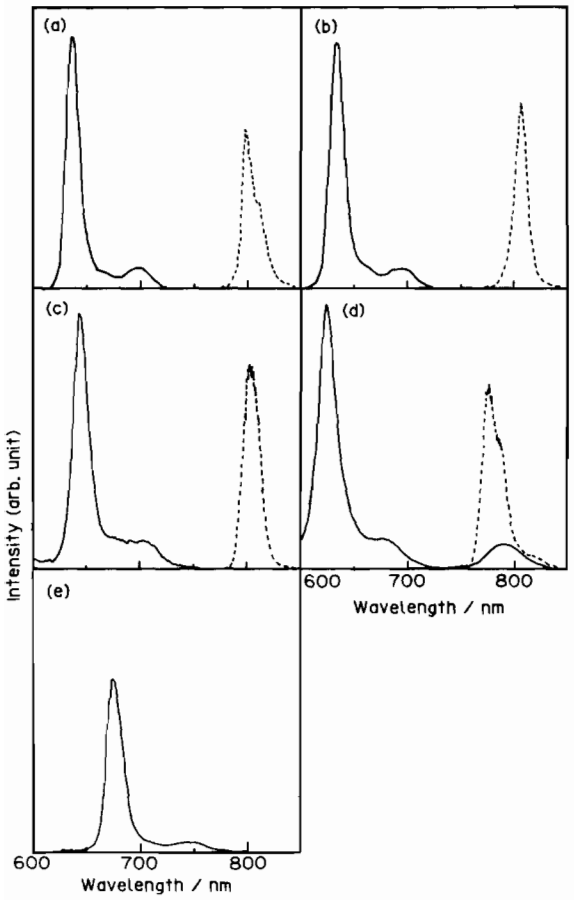

Fig. 7. A series of emission spectra of P_2TBPs. The solid lines represent the fluorescence spectra at room temperature and the dashed lines indicate the phosphorescence spectra in the deoxygenated EPA glasses at 77 K. (a) MgP_2TBP, (b) ZnP_2TBP, (c) CdP_2TBP, (d) PdP_2TBP, (e) H_2P_2TBP.

as listed in Table 4. On the other hand, the treatment of this relationship for the second singlet excited states (Soret band absorption) reveals that the f_S decreases with increasing the energies (E_S), as shown in Fig. 6. Although the reason for the previous results in unclear, the central metal ions have an influence on the absorption properties of the P_2TBPs as well as on the redox properties, probably based on the induction effect of the metal ions on the porphyrin π-electron system.

Figure 7 shows a series of the emission spectra of the P_2TBPs including both fluorescence at room temperature and phosphorescence at 77 K. The fluorescence spectra keep the mirror images against the absorption ones so that the singlet excitation energies ($^*E_{00}$) are derived from the point of intersection of the singlet excitation (absorption) and emission spectra. The metallo P_2TBPs have a singlet energy of about 44–46 kcal mol^{-1} (1.91–1.99 eV), while H_2P_2TBP possesses a slightly lower energy of 42.4 kcal mol^{-1} (1.84 eV) (Table 5). This is due to the location of its Q band, which splits into $Q_x(0,0)$ and $Q_y(0,0)$ as a consequence of the weakened symmetry of the porphyrin π-cloud from D_{4h} to D_{2h}, in the far long wavelength region (λ_{max} = 672 nm in benzene) in comparison with the metal complexes. The peak tops of the phosphorescence spectra recorded in the frozen EPA glasses give their triplet energies ranging from 35 to 37 kcal mol^{-1}. The Pd complex gives a weak phosphorescence even at room temperature. The phosphorescence spectrum was not observed for H_2P_2TBP probably on account of the wavelength limit (<850 nm).

The fluorescence lifetimes (τ_f) of **1a**, **1b** and **1e** were measured at 20 °C in *c.* 10^{-6} M benzene solutions prepared thorough purging with argon gas, using a time-correlated single photon counting method. Figure 8 shows the time profiles of the fluorescence of these compounds. In the case of both the Cd (**1c**) and the Pd (**1d**) complexes, the lifetimes were so short that they had to be measured with nano-second single-photon counting equipment. The lifetimes decrease in the following order; H_2P_2TBP (12.60 ns) > MgP_2TBP (7.41 ns) > ZnP_2TBP (1.33 ns). This is due to the heavy atom effect by the central metals, as in the case of TPPs [13]. The fluorescence quantum yields (Φ_f) relative to that for ZnTPP obtained by the Soret band excitation are given in benzene solutions to be 0.22 for **1e**, 0.48 for **1a**, 0.16 for **1b**, 7.7×10^{-3} for **1c** and 4.0×10^{-4} for **1d**. Except for **1e**, the Φ_fs for these metallo P_2TBPs decrease with an increase of the heavy atom effect by the central metals. Assuming that the sum of Φ_f and Φ_{isc} (intersystem crossing quantum yield) is nearly unity as in the case of TBP [14] and TPP [15], their Φ_{isc} are estimated form $1-\Phi_f$. By use of these simple photophysical parameters (τ_f, Φ_f and Φ_{isc}), the other parameters such as k_f and k_{isc}, are approximately estimated from the simple calculations, $k_f = \Phi_f/\tau_f$ and

TABLE 5. Absorption and emission data of the zero–zero bands for P_2TBPs, and the calculated excited state energies

Compound	Absorption and emission data (nm)			Energy (kcal mol^{-1})	
	Q(0,0)[a]	Q(0,0)[a]	T(0,0)[b]	E_S	E_T
MgP_2TBP (**1a**)	629	633	800	45.2	35.7
ZnP_2TBP (**1b**)	630	634	806	45.2	35.4
CdP_2TBP (**1c**)	636	638	804	44.8	35.5
PdP_2TBP (**1d**)	615	624	775	46.1	36.8
H_2P_2TBP (**1e**)	672	675		42.4	

[a]Obtained in benzene solutions. [b]Obtained in deoxygenated EPA glasses at 77 K.

TABLE 6. Photophysical properties of P_2TBPs

Compound	τ_f (ns)[a]	Φ_f[a,b]	k_f (10^8 s^{-1})[c]	Φ_{isc}[d]	k_{isc} (10^8 s^{-1})[e]
H_2P_2TBP (**1e**)	12.60	0.22	0.18	0.78	0.62
MgP_2TBP (**1a**)	7.41	0.48	0.65	0.52	0.70
ZnP_2TBP (**1b**)	1.33	0.16	1.20	0.84	6.32
CdP_2TBP (**1c**)	ND	7.7×10^{-3}		*c.* 1	
PdP_2TBP (**1d**)	ND	4.0×10^{-4}		*c.* 1	

[a]Measured in the optically diluted benzene solutions (10^{-6} M) after thorough purging with argon gas. [b]Relative to $\Phi_f=0.033$ of ZnTPP from ref. 8. [c]Calculated from Φ_f/τ_f. [d]Estimated from $1-\Phi_f$. [e]Calculated form Φ_{isc}/τ_f.

TABLE 7. Ground and excited state redox potentials (eV vs. SCE) for P_2TBPs and ZnTPP in DMF

Compound	$E(M^+/M)$	$E(M^+/{}^*M^1)$	$E(M^+/{}^*M^3)$	$E(M/M^-)$	$E({}^*M^1/M^-)$	$E({}^*M^3/M^-)$
MgP_2TBP (**1a**)	0.40	−1.56	−1.15	−1.54	0.42	0.01
ZnP_2TBP (**1b**)	0.53	−1.43	−1.01	−1.44	0.52	0.10
CdP_2TBP (**1c**)	0.54	−1.39	−1.00	−1.44	0.49	0.10
PdP_2TBP (**1d**)	0.74	−1.26	−0.86	−1.27	0.73	0.33
H_2P_2TBP (**1e**)	0.72	−1.13		−1.18	0.67	
ZnTPP	0.86	−1.20	−0.73[a]	−1.35	0.71	0.24[a]

[a]Triplet energy for ZnTPP from ref 2.

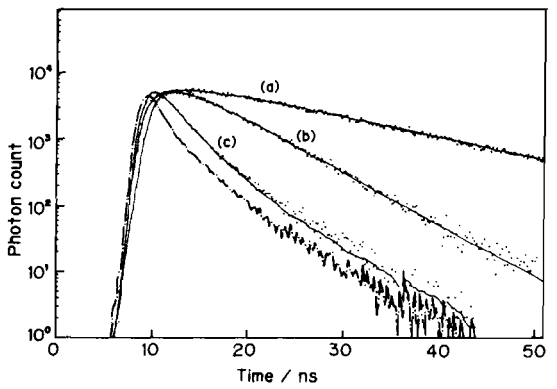

Fig. 8. Time profiles of the fluorescences of: (a) H_2P_2TBP, (b) MgP_2TBP, (c) ZnP_2TBP in the optically diluted benzene solutions (10^{-6} M) prepared by thorough purging with argon gas, using a time-correlated single-photon counting equipment (HORIBA NAES-1100). These decay curves were obtained by the excitation of the Soret bands. The emissions above 600 nm were collected by use of KENKO R60 colour filter.

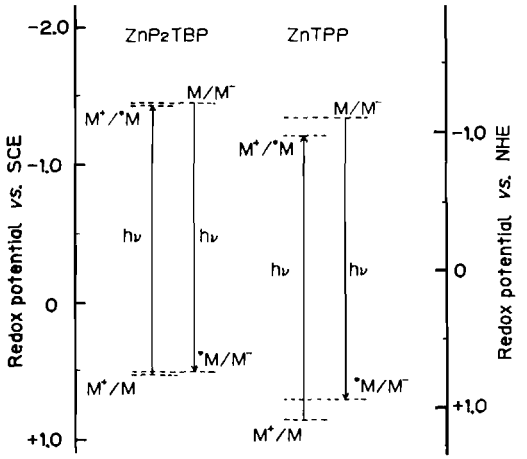

Fig. 9. Schematic representation for the redox potentials of the ground and excited states of ZnP_2TBP and ZnTPP according to eqns. (1) and (2). Both M^+ and M^- stand for the states of the molecules either oxidized or reduced by one-electron. *M indicates the excited state of molecule and $h\nu$ corresponds to the zero–zero spectroscopic energy of the excited state. All of the data were obtained in DMF solutions.

$k_{isc}=\Phi_{isc}/\tau_f$, respectively. The sum of their photophysical properties are listed in Table 6.

Redox properties in excited states

Finally, we investigated the redox properties of P_2TBP in the excited states. It is well known that the change in shape, size and solvation of the excited state molecule with regard to the ground state one affects the Stokes shift between absorption and emission [16]. When the Stokes shift is small, the changes are also presumed to be small, so that the difference in the entropy content between the two states may be negligible. The TBPs discussed here are such cases. In such a case, the redox potentials of the excited state are approximately determined by the following equations [17]

$$E(M^+/{}^*M)=E(M^+/M)-E_{00}(M\text{-}{}^*M) \quad (1)$$

$$E(^*M/M^-) = E(M/M^-) + E_{00}(M\text{-}^*M) \quad (2)$$

where $E(M^+/M)$ and $E(M/M^-)$ are the redox potentials in the ground state, $E(M^+/^*M)$ and $E(^*M/M^-)$ are those for the excited state. $E_{00}(M\text{-}^*M)$ stands for the one-electron potential corresponding to the zero–zero spectroscopic energy of the excited state. Generally, eqns. (1) and (2) are used to obtain an estimate of excited state redox potential.

Table 7 summarizes the calculated values by use of the previous redox data in ground states and their excited energies in DMF. The comparison of ZnP_2TBP with ZnTPP with respect to these properties indicate that the former are more susceptible to oxidation than the latter, as demonstrated in Fig. 9.

Conclusions

The measurement of the redox properties of the divalent metallo P_2TBPs (**1a–1d**) has revealed that their redox potentials increase with increasing electronegativities of the central metals. This result is explained on the basis of the induction effect of the metals on the porphyrins π-electron system. These metallo P_2TBPs possess Q band absorptions with high extinction coefficients of above 10^5 in the red-light region. Although the absorption maxima of their Q bands vary with the central metals, there is no relationship between the oscillator strength (f_Q) and the energy (E_Q) of the Q band to interpret the shifts of the bands. On the other had, their f_{Soret}s decrease with increasing their E_{Soret}s.

Since these P_2TBP fluoresce and phosphoresce at room temperature and at 77 K, respectively, both the singlet and triplet excited energies are obtainable. The central metals affect the fluorescence quantum yields and lifetimes on account of the heavy atom effect, as in the case of the TPPs. Comparing the oxidation properties of ZnP_2TBPs in the photoexcited states with those of ZnTPP, the former is expected to serve as an efficient electron donor in the photoexcited state because of its low oxidation potentials in the excited state. Hence, this unique character would be expected to be available as an electron donor for photoinduced electron transfer reaction.

Acknowledgement

We thank Dr Sei-ichiro Iijima of the Research Institute for Polymers and Textiles for the CV measurements and the helpful discussions.

References

1 D. Dolphin (ed), *The Porphyrins,* Vols. 1–7, Academic Press, New York, 1978.
2 K. M. Smith (ed.), *Porphyrins and Metalloporphyrins,* Elsevier, Amsterdam, 1975.
3 B. D. Berezin (ed.), *Coordination Compounds of Porphyrins and Phthalocyanines,* Wiley, New York, 1981.
4 (a)M. Gouterman, in D. Dolphin (ed.), *The Porphyrins,* Vol. 3, Part A, Academic Press, New York, 1978, p. 21; (b) O. N. Korotaev, E. I. Donskoi and V. I. Glyadkovskii, *Opt. Spectrosc., 59* (1985) 492.
5 (a) A. Vogler, B. Rethwisch, H. Kunkely, J. Huttermann and J. Besenhard, *Angew. Chem., Int. Ed. Engl., 17* (1978) 951; (b) J. C. Goedheer, *Photochem. Photobiol., 6* (1967) 521.
6 (a) V. N. Kopranenkov, S. N. Dashkevich and E. Ya. Lykyanets, *Zh. Obshch. Khim.,* 51 (1985) 2513; (b) V. N. Kopranenkov, E. A. Makarova and S. N. Dashkevich, *Khim. Geterotsikl. Soedin.,* (1985) 1372; (c) D. E. Remy, *Tetrahedron Lett., 24* (1983) 1452; (d) K. Ichimura, M. Sakuragi, H. Morii, M. Yasuike, Y. Toba, M. Fukui and O. Osamu, *Inorg. Chim. Acta, 186* (1991) in press.
7 (a) K. Ichimura, M. Sakuragi, H. Morii, M. Yasuike, M. Fukui and O. Ohno, *Inorg. Chim Acta, 176* (1990) 31; (b) *182* (1991) 83.
8 D. J. Quimby and F. R. Longo, *J. Am. Chem. Soc., 97* (1975) 5111.
9 (a) R. H. Felton, in D. Dolphin (ed.), *The Porphyrins,* Vol. 5, *Physical Chemistry,* Part C, Academic Press, New York, 1978, p. 53; (b) D. G. Davis, p. 127.
10 A. Stanienda, *Z. Naturforsch, Teil B, 23* (1968) 1285.
11 J. H. Furhop, K. M. Kadish and D. G. Davis, *J. Am. Chem. Soc., 95* (1973) 5140.
12 D. Lexa and M. Reix, *J. Chim. Phys. Physisochim. Biol., 71* (1974) 511.
13 (a) M. Gouterman, in D. Dolphin (ed.), *The Porphyrins,* Vol. 3, Part A, Academic Press, New York, 1978, p. 1; (b) A. Harriman, *J. Chem. Soc., Faraday Trans. 2, 77* (1981) 1281; (c) J. R. Darwent, P. Douglas, A. Harriman, G. Porter and M. C. Richoux, *Coord. Chem. Rev., 44* (1982) 83.
14 A. T. Gradyushko, A. N. Sevchenko, K. N. Solovyov and M. P. Tsuvirko, *Photochem. Photobiol., 11* (1970) 387.
15 K. Kikuchi, Y. Kurabayashi, H. Kokubun, Y. Kaizu and H. Kobayashi, *J. Photochem. Photobiol. A: Chem., 45* (1988) 261.
16 (a) G. A. Crosby, *Acc. Chem. Res., 8* (1975) 231; M. K. DeArmond, *Acc. Chem. Res. 7* (1974) 309.
17 V. Balzani, F. Bolletta, M. T. Gandolfi and M. Maestri, *Topics in Current Chemistry,* Vol. 75, Springer, Berlin, 1978, p. 1.